The Effect of Denoising on Superresolution of Hyperspectral Imaging

Armin Eskandari[a] and Azam Karami[a,b]

[a]Faculty of Physics, Shahid Bahonar University of Kerman, Iran;
[b]Vision Lab, University of Antwerp, Belgium;

ABSTRACT

Hyperspectral Images (HSI) are usually affected by different type of noises such as Gaussian and non-Gaussian. The existing noise can directly affect the classification, unmixing and superresolution analyses. In this paper, the effect of denoising on superresolution of HSI is investigated. First a denoising method based on shearlet transform is applied to the low-resolution HSI in order to reduce the effect of noise, then the superresolution method based on Bayesian sparse representation is used. The proposed method is applied to real HSI dataset. The obtained results of the proposed method in comparison with some of the state-of-the-art superresolution methods show that the proposed method significantly increases the spatial resolution and decreases the noise effects efficiently.

Keywords: Superresolution, Sparse representation, Shearlet Transform

1. INTRODUCTION

Nowadays HSI have been used in many practical applications such as mining, agriculture, astronomy and etc. The spectral resolution of HSI is higher than multispectral images (MSI), this means that classification or unmixing analysis, using HSI instead of MSI leads to more precise results. However, the spectral resolution of HSI is higher than MSI, because of sensor limitations its spatial resolution is not significant. In order to solve this problem, different superresolution methods have been introduced recently. Most of the superresolution methods are based on the fusion of HSI with high spatial resolution images such as MSI. These fusion methods can be generally divided into two main groups: spectral unmixing based and sparse representation based approaches.

For example, an efficient method based on sparse representation is introduced in.[1] In this method, a Bayesian sparse (BS) concept is used. First, the principal component analysis (PCA) is applied to the existing low-resolution HSI (LRHSI) in order to reduce the spectral dimensionality. After that, a proper dictionary is constructed using LRHSI and MSI. Then, the superresolution problem is solved using an alternative optimization problem. The other sparse representation based fusion is introduced in.[2] This method considers the non-local self-similarity of spectra. In this method a spectral dictionary is constructed from LRHSI and similar pixels in MSI are grouped first, and after that a spatial dictionary is created. Finally, high-resolution HSI (HRHSI) is produced using an iterative back-projection method.

In spectral unmixing (SU) based fusion methods, the original images are decomposed into endmember and abundance fraction matrices.[3] The endmember matrix is extracted from the LRHSI and the abundance fractions are estimated from MSI. One of the popular method is coupled non-negative matrix factorization (CNMF).[4] It is applied in order to alternately update the abundance fractions from the MSI and the endmember spectra from the LRHSI. Another example is a fusion method based on unsupervised spectral unmixing.[5] In this method, the ill-posed fusion problem is solved by maximizing the joint posterior distribution with respect to endmembers and abundance fractions.

Recently a superresolution method based on the combination of spectral unmixing and sparse coding (SUSC)[6] is introduced. This method shows better performance than the spectral unmixing[7] and sparse coding[8] methods. Superresolution using spectral unmixing and Bayesian sparse representation (SUBS)[9] is another example of

Further author information: (Send correspondence to Azam Karami)
Azam Karami: E-mail: akarami@uk.ac.ir, Telephone: +98 34 3325 7258

Image and Signal Processing for Remote Sensing XXIII, edited by Lorenzo Bruzzone, Francesca Bovolo
Proc. of SPIE, Vol. 10427, 1042708 · © 2017 SPIE · CCC code: 0277-786X/17/$18 · doi: 10.1117/12.2278503

combination methods. In this method, spectral unmixing is applied to extract the endmember matrix from LRHSI and the abundance fraction are obtained from MSI by solving an optimization fusion problem.

Due to the sensor limitation, the LRHSI are affected by different type of noises e.g. Gaussian noise and non-Gaussian such as Spike noise (salt-and-pepper noise). Atmospheric absorption and instrumental noise create Gaussian noise. Moreover, for most sensors the Gaussian noise power varies among bands. Spike noise appears when the sensors have unpredictable calibration.[10] The existing noise causes the degradation of HSI and hinders the effectiveness of subsequent HSI processing task, e.g. fusion, spectral unmixing,[11] classification[12] and segmentation.[13] HSI denoising is a well-studied problem. For example[14][15] remove the mixture of Gaussian and Spike noises.

Recently we introduced a noise reduction method for HSI based on shearlet transform (ST).[16] In this method, first, the bands are divided into two groups: bands dominated by low-level noise (LN) and bands containing mixed noise (MN) such as high-level Gaussian noise and Spike noise, based on the spectral correlation. After that 2D shearlet transform is applied to all bands. The LN bands are denoised using Bayesian thresholding and the effect of noise in MN bands are reduced using the details information of shearlet transform coefficients from neighboring LN bands.

In this paper because the adverse effect of MN is stronger than LN, therefore we investigated the effect of noise reduction of high-level noise on fusion of LRHSI and MSI by using a combination of ST and BS, the proposed method (STBS) simultaneously decreases the effect of noise and increases the spatial resolution. The proposed method is applied to real HSI and MSI dataset and compared with the spectral unmixing base method CNMF,[4] the sparse representation method BS[1] and the combined method SUSC.[6]

The rest of this paper is organized as follows. In Section 2, the proposed algorithm is described. Section 3 presents the experimental results and Section 4 concludes the paper.

2. PROPOSED METHOD

In this section first we give the definitions and notations used throughout the paper. In this paper, tensors are donated by capitalized and calligraphic letters e.g. $\mathcal{A}$. Matrices are denoted by capitalized boldface letters, e.g. $\boldsymbol{A}$. Vectors are denoted by boldface lower-case letters e.g. $\boldsymbol{a}$. Scalars are denoted by lower-case letters e.g. a. The proposed method (STBS) is explained in detail in the following:

2.1 Shearlet transform

Classical wavelets are popular to create an optimal approximation but do not optimally represent multivariate functions such as images that are typically included anisotropic features such as edges. Recently shearlet transform has been introduced. It can optimally provide sparse representation for a large class of multidimensional data and guide to improvement in many image processing such as denoising[16] and image fusion.[17]

In this paper, a special type of discrete shearlet transform is used, called non-subsampled shearlet transform (NSST). This transform is shift invariant and well known in image denoising. The NSST contains two main steps. First: non-subsampled pyramid (NSP) filter banks. These filters do not include any upsampling and downsampling filters. In fact, the NSP filter banks create a multiscale decomposition of the original image into high-frequency subbands and low-frequency subbands. Second: non-subsampled shearing (NSS) filter banks accomplish the directional filtering in the spatial domain. The NSS decomposes the high-frequency subbands into directional subbands. The filter banks are iteratively applied. At each iteration, the obtained low-frequency subband is again decomposed into a lower scale high-frequency and low-frequency subbands (see[16] for more details).

LRHSI data contaminated by mixed noise are denoted by $\mathcal{Y}_{\mathcal{H}} \in \mathbb{R}^{i_1 \times i_2 \times b_h}$ where $(i_1 \times i_2)$ are the total number of pixels in the spatial direction of LRHSI. b_h is the number of spectral bands of LRHSI. LRHSI can be modeled as:

$$\mathcal{Y}_{\mathcal{H}} = \mathcal{Z} + \mathcal{S} + \mathcal{N}_{\mathcal{H}} \tag{1}$$

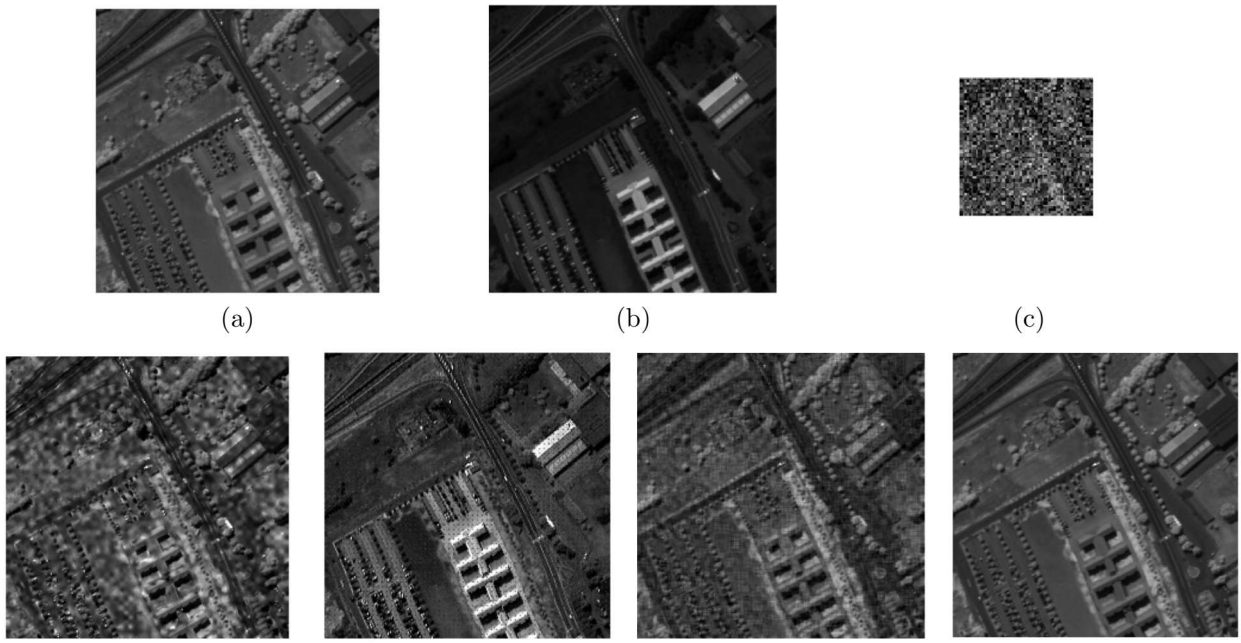

Figure 1: (a) Band 82 of the Pavia groundtruth image. (b) First band of MSI. (c) Noisy band 82 of LRHSI; Band 82 of HRHSI obtained by: (d) CNMF; (e) SUSC; (f) BS; (g) Proposed method (STBS)

where $\mathcal{Z} \in \mathbb{R}^{i_1 \times i_2 \times b_h}$ is the clean LRHSI, $\mathcal{S} \in \mathbb{R}^{i_1 \times i_2 \times b_h}$ and $\mathcal{N}_{\mathcal{H}} \in \mathbb{R}^{i_1 \times i_2 \times b_h}$ are sparse noise and Gaussian noise respectively. The spares noise includes non-Gaussian noise. In fact, sparse noise refers to the noise which corrupts only a few pixels in the image with strong level.

As it is mentioned the impact of denoising of high-level noise on fusion of HSI and MSI is very important. In the denoising procedure using shearlet transform first the images are divided into LN and MN bands based on spectral correlation. The LN bands are denoised using BayesShrink thresholding. After that, the recovered shearlet coefficients of adjacent bands are fused into MN detail subbands.

In this paper first the effect of high Gaussian noise on fusion of HSI and MSI is investigated. Second, we also added Spike noise with level $\frac{d}{2}$ as a sparse noise, where d is the probability that reflectance value changes to zero or one.

After denoising the existing LRHSI, an efficient fusion method "BS" is applied to MSI and LRHSI. This fusion process will be explained in the following.

2.2 BS fusion

The clean LRHSI ($\mathcal{Z}$) in Eq.1 can be considered as a blurred and downsampled of HRHSI. In fact, LRHSI have high-spectral and low-spatial resolutions. It can be modeled as follows:[18]

$$\boldsymbol{Z} = \boldsymbol{YBD}; \boldsymbol{Z} \in \mathbb{R}^{b_h \times n_h}, \boldsymbol{Y} \in \mathbb{R}^{b_h \times n}, \boldsymbol{B} \in \mathbb{R}^{n \times n}, \boldsymbol{D} \in \mathbb{R}^{n \times n_h} \tag{2}$$

where n_h is the total number of LRHSI pixels ($n_h = i_1 \times i_2$); n is the total number of HRHSI pixels; $\boldsymbol{Y}$ is the HRHSI; $\boldsymbol{B}$ is a spatial blurring matrix; $\boldsymbol{D}$ is a downsampling matrix;

The Eq.2 substitutes in Eq.1, in this case we will have:

$$\boldsymbol{Y_H} = \boldsymbol{YBD} + \boldsymbol{S} + \boldsymbol{N_H}; \boldsymbol{Y_H} \in \mathbb{R}^{b_h \times n_h}, \boldsymbol{S} \in \mathbb{R}^{b_h \times n_h}, \boldsymbol{N_H} \in \mathbb{R}^{b_h \times n_h} \tag{3}$$

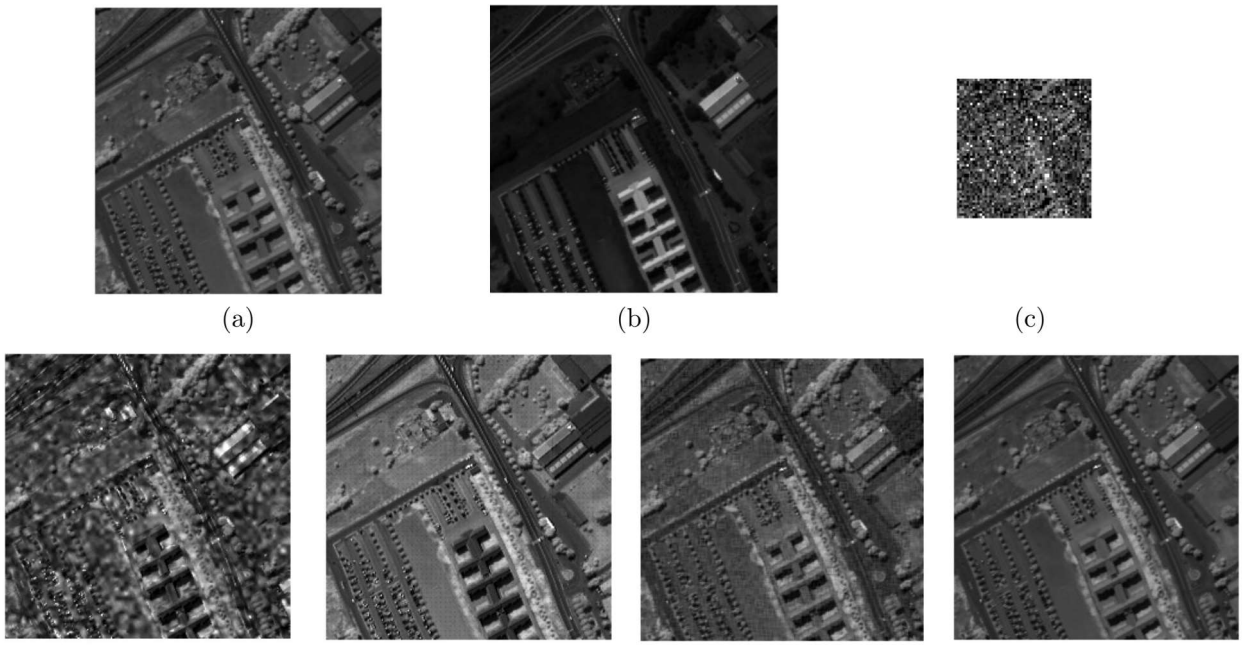

Figure 2: (a) Band 76 of the Pavia groundtruth image. (b) First band of MSI. (c) Noisy band 76 of LRHSI; Band 76 of HRHSI obtained by: (d) CNMF; (e) SUSC; (f) BS; (g) Proposed method (STBS)

It is noteworthy to mention that $\boldsymbol{Z}$, $\boldsymbol{Y_H}$, $\boldsymbol{S}$, $\boldsymbol{N_H}$ in Eq.2 & 3 are denoted the matrix version of these symbols in comparison with Eq.1.

Assume that MSI from the same scene of LRHSI is also available and co-registered. MSI usually have high-spatial and low-spectral resolutions. MSI can be considered as follows:

$$\boldsymbol{Y_M} = \boldsymbol{RY} + \boldsymbol{N_{MS}}; \boldsymbol{Y_M} \in \mathbb{R}^{b_m \times n_m}, \boldsymbol{R} \in \mathbb{R}^{b_m \times b_h}, \boldsymbol{N_{MS}} \in \mathbb{R}^{b_m \times n_m}; n_m \gg n_h; b_m \ll b_h \tag{4}$$

where $\boldsymbol{Y_M}$ is MSI; $\boldsymbol{R}$ is the spectral response of the multispectral sensor; $\boldsymbol{N_{MS}}$ is additive Gaussian noise; n_m is the total number of pixels in MSI which is equal to HRHSI ($n_m = n$); b_m is the number of MSI bands.

As it is mentioned the MN noise degrades the HSI a lot and the BS fusion method is sensitive to the existing noise. Therefore, the noisy LRHSI ($\boldsymbol{Y_H}$) first is denoised by NSST:[16]

$$\widetilde{\boldsymbol{Y_H}} = NSST(\boldsymbol{Y_H}) \tag{5}$$

It is noteworthy to mention that the effect of $\boldsymbol{N_{MS}}$ in comparison to $\boldsymbol{N_H}$ is negligible. Therefore, the NSST is only applied to $\boldsymbol{Y_H}$. After that the BS fusion method is applied to $\widetilde{\boldsymbol{Y_H}}$ and $\boldsymbol{Y_M}$.

As it is mentioned HSI are generally spectrally dependent and can be projected into lower spectral dimension. The following model for HRHSI ($\boldsymbol{Y}$) can be considered:[1]

$$\boldsymbol{Y} = \boldsymbol{HU}; \boldsymbol{H} \in \mathbb{R}^{b_h \times b_h^{'}}, \boldsymbol{U} \in \mathbb{R}^{b_h^{'} \times n_m}, b_h^{'} \ll b_h \tag{6}$$

where $\boldsymbol{H}$ is an orthogonal matrix, $\boldsymbol{U}$ is the projection of matrix $\boldsymbol{Y}$ onto the subspace spanned by the columns of matrix $\boldsymbol{Y}$. By replacing the Eq.6 into Eqs.3 & 5 we will have:

$$\widetilde{\boldsymbol{Y_H}} \approx \boldsymbol{HUBD} \tag{7}$$

$$\boldsymbol{Y_M} = \boldsymbol{RHU} + \boldsymbol{N_{MS}} \tag{8}$$

In this paper $\boldsymbol{H}$ is first obtained by applying PCA to $\boldsymbol{Y_H}$ and it is considered as constant. Now the $\boldsymbol{U}$ matrix should be estimated from LRHSI and MSI. A rough estimation for $\boldsymbol{U}$ can be calculated using $\widetilde{\boldsymbol{Y_H}}$ and $\boldsymbol{Y_M}$ (see[19] for more details). After that the maximum a posterior (MAP) estimator of $\boldsymbol{U}$ using an optimization framework to solve the fusion problem is considered. The mentioned optimization problem is usually an ill-posed inverse problem which requires a regularization term in order to convert it into a well-posed inverse problem. Sparse coding (SC) is used as a regularizer. In SC, the dictionary is constructed from existing LRHSI and MSI using online dictionary learning (ODL).[20] The sparse code matrix is calculated by orthogonal matching pursuit.[21] After that the $\boldsymbol{U}$ and SC matrices are obtained through an interactive optimization method. In this case the optimization with respect to (w.r.t.) $\boldsymbol{U}$, conditional on SC can be efficiently solved with the split augmented Lagrangian Shrinkage algorithm (SALSA).[22] The optimization w.r.t. sparse code conditional on $\boldsymbol{U}$ can be easily computed using least square (LS) regression (see[7] for more details). The pseudo code of the proposed algorithm is briefly given by Algorithm.1.

Algorithm 1 STBS method

Input: $\boldsymbol{Y_H}$, $\boldsymbol{Y_M}$, $\boldsymbol{B}$, $\boldsymbol{D}$, *dictionary parameters*

1. Denoise $\boldsymbol{Y_H}$ using NSST $\Longrightarrow \widetilde{\boldsymbol{Y_H}} = NSST(\boldsymbol{Y_H})$;
2. Fusion $(\widetilde{\boldsymbol{Y_H}}, \boldsymbol{Y_M})$ using BS;

Output: HRHSI($\boldsymbol{Y}$)

3. EXPRIMENTAL RESULTS

3.1 Quality Metrics

In order to validate the quality of the obtained HRHSI ($\mathcal{Y}$), four image quality measurements have been calculated, based on the comparison with the high-resolution groundtruth HSI ($\mathcal{Y}_{\mathcal{G}}$)

1. The peak signal-to-noise ratio (PSNR) which measures the power of reconstructed signal.

$$PSNR = \frac{\sum_{i=1}^{b_h} 10log_{10}(\frac{Max_i^2}{MSE_i})}{b_h}$$

$$MSE = \frac{1}{n_m}\sum_{j=1}^{n_m}(y_{G_{i,j}} - y_{i,j})^2 \tag{9}$$

Where Max_i is the maximum value of the i_{th} band; $y_{G_{i,j}}$ and $y_{i,j}$ are the j_{th} pixel of the i_{th} band of groundtruth and reconstructed image respectively.

2. The spectral angular mapper (SAM) which measures the spectral distortion of the final result in comparison with groundtruth.

$$SAM = \frac{1}{n_m}\sum_{j=1}^{n_m} arccos(\frac{\boldsymbol{y}_{:,j}, \boldsymbol{y}_{G_{:,j}}}{||\boldsymbol{y}_{:,j}||_2||\boldsymbol{y}_{G_{:,j}}||_2}) \tag{10}$$

where $\boldsymbol{y}_{G_{:,j}}$ and $\boldsymbol{y}_{:,j}$ is the spectrum of the j_{th} pixel of the groundtruth and reconstructed image respectively.

3. The error relative global-dimensional synthesis index (ERGAS) which measures the spectral distortion of reconstructed HSI (HRHSI).

$$ERGAS = 100\frac{1}{k}\sqrt{\frac{1}{b_h}\sum_{i=1}^{b_h}\frac{MSE(\boldsymbol{y}_{i,:}, \boldsymbol{y}_{G_{i,:}})}{\mu^2_{y_{G_{i,:}}}}} \tag{11}$$

where k is the ratio the spatial resolution between LRHSI and high-resolution MSI; $\boldsymbol{y}_{G_{i,:}}$ and $\boldsymbol{y}_{i,:}$ are the i_{th} band of groundtruth and reconstructed image respectively; $\mu_{y_{G_{i,:}}}$ is the mean of $\boldsymbol{y}_{G_{i,:}}$

4.The cross correlation (CC), which is a parameter to measure the spatial distortion.

$$CC = \frac{1}{b_h}\sum_{i=1}^{b_h} CCS(\boldsymbol{y}_{G_{i,:}}, \boldsymbol{y}_{i,:})$$

$$CCS = \frac{\sum_{j=1}^{n_m}(y_{G_{i,j}} - \mu_{y_{G_{i,:}}})(y_{i,j} - \mu_{y_{i,:}})}{\sqrt{\sum_{j=1}^{n_m}(y_{G_{i,j}} - \mu_{y_{G_{i,:}}})^2 (y_{i,j} - \mu_{y_{i,:}})^2}} \tag{12}$$

where $\mu_{y_{i,:}}$ is the mean of $\boldsymbol{y}_{i,:}$.

3.2 Real Datasets

The proposed method (STBS) has been applied to a real HSI dataset. This dataset was acquired by the reflective optics system imaging spectrometer (ROSIS) optical sensor over the urban area of the university of Pavia, Italy*. The image size is $610 \times 340 \times 115$. The water absorption bands [1-10] and [104-115] are removed and 93 bands are retained. For simulation, groundtruth subimage is selected with size $240 \times 240 \times 93$. For this dataset, MSI of the same scene does not exist. Therefore, MSI of four bands is generated by filtering the HSI with the IKONOS-like reflectance responses which is scaled with size $240 \times 240 \times 4$. An LRHSI has been constructed by applying a 5×5 Gaussian spatial filter with $\sigma = 2.5$ of spatial directions to each band of groundtruth HSI and downsampling by a factor of four in both horizontal and vertical directions this leading to a LRHSI with size $60 \times 60 \times 93$.

3.3 Parameter Setting

In order to investigate the effect of denoising on fusion process, first high Gaussian noise is randomly added to 30 spectral bands of LRHSI. To obtain variable noise from band to band, the standard deviation σ are randomly chosen with the interval [0.2, 0.4]. Second, the Spike noise (non-Gaussian) with level $\frac{d}{2}$ is added to the previous noisy bands. Where d is the probability that a reflectance value changes to zero or one, was taken in the interval $0.2 \leqslant d \leqslant 0.4$ for each band. In order to denoise, NSST with three level decomposition is used and the number of shearing direction is chosen to be 16,8 and 4 at scales 1, 2, 3 respectively.

In BS fusion method, the value of λ has been set empirically to 25. For the ODL algorithm in this paper 3481 patches of size 6×6 are used, and the number of atoms is 256. The proposed algorithm (STBS) is compared to the following algorithm the spectral unmixing based fusion method CNMF,[4] the sparse representation based fusion BS,[1] combined method SUSC.[6] In CNMF, the maximum number of iterations in the linear and outer loops are selected as 100 and 1 respectively. In SUSC, the patch size is 8×8; The number of atoms is 332 and λ is 1.

3.4 Fusion Results

The proposed method is compared with some of the state-of-the-art algorithms. Table.1 displays quality measures for high-level Gaussian and mixed noises. The fusion results obtained from different algorithms are depicted in Figures.1, 2 for both noises (Bands 82 and 76 are affected by high Gausssian noise and Spike noise respectively). From the obtained results, it can be seen that the proposed approach outperforms than the other fusion methods.

The reconstructed images by the proposed method (STBS) are visually very close to the groundtruth. As it shown in Table.1 the superior performance of the proposed method can be contributed to an improve spatial resolution (high PSNR and CC values) and decrease spectral distortion (low SAM and ERGAS values) compared to the CNMF, SUSC and BS methods. In fact, CNMF couldn't remove the noise effect (especially mixed noise). It would appear that the fused image by the SUSC contains more noise than BS. Moreover, it is clearly seen that the proposed denoising-fusion (STBS) method remove the noise as much as possible while preserving the important spatial information such as edges very well and as it is shown the fusion quality is also visually better than other methods.

The algorithms computed on a system with Intel(R) Core(TM) i7 CPU (3.60 GHz), 64 GB RAM, 64-bit operating system. All computing times for the proposed method and the other algorithm are also calculated.

*[Online]. Available: http://www.ehu.eus/ccwintco/index.php?title=Hyperspectral_Remote_Sensing_Scenes

Table 1: Quality indices for obtained fusion results induced by different type of noises

Methods	High Gaussian noise				Mixed noise				*Time*$_{(s)}$
	PSNR (*dB*)	*SAM* (*rad*)	*ERGAS*	*CC*	*PSNR* (*dB*)	*SAM* (*rad*)	*ERGAS*	*CC*	
CNMF[4]	32.45	0.320	9.62	0.896	33.53	0.334	19.73	0.884	**9.92**
SUSC[6]	32.11	0.246	14.69	0.924	30.80	0.277	11.63	0.925	156.98
BS[1]	35.49	0.125	3.44	0.979	33.34	0.151	4.01	0.971	56.85
STBS	**41.81**	**0.069**	**2.28**	**0.987**	**40.34**	**0.040**	**1.33**	**0.996**	56.09

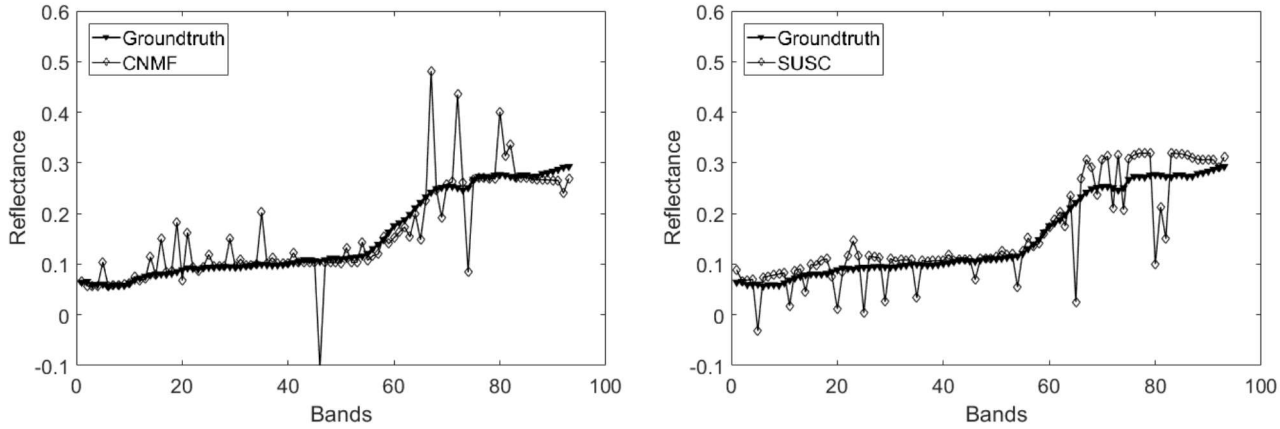

(a) CNMF

(b) SUSC

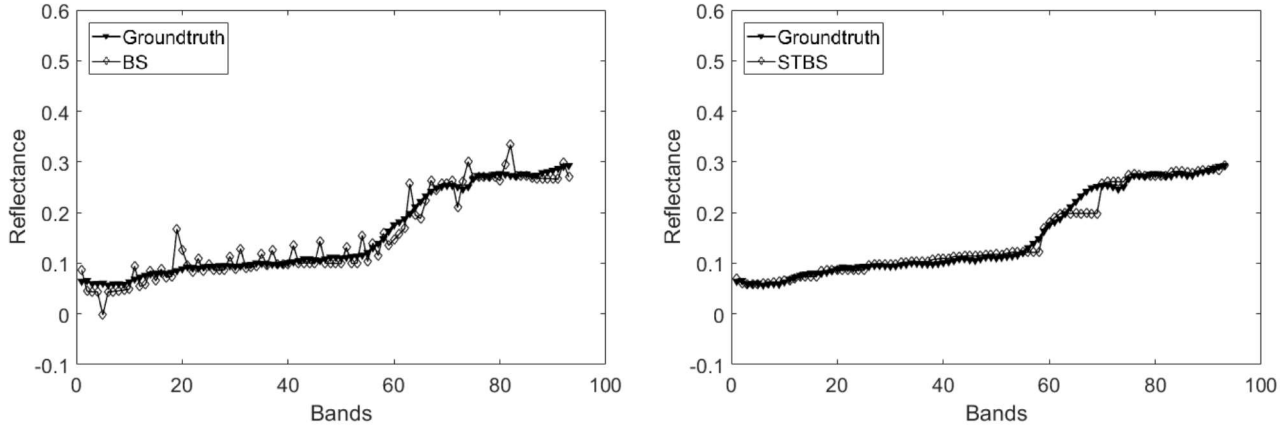

(c) BS

(d) STBS

Figure 3: Reconstructed spectrum using different fusion methods (high Gaussian noise)

The required computing time for the proposed method is close to BS and the CNMF takes the lowest time. SUSC requires a considerable amount of time.

Figures.3 & 4 show the spectra pixel [10, 1] (it is the spectrum of meadows) in the ground truth and reconstructed images. The spectral distortion value is the lowest in the proposed method. Therefore, the reconstructed HRHSI have simultaneously a high spatial and spectral resolutions compared to the other methods.

In order to demonstrate the effect of the denoising and fusion on further analysis, the impact of the proposed

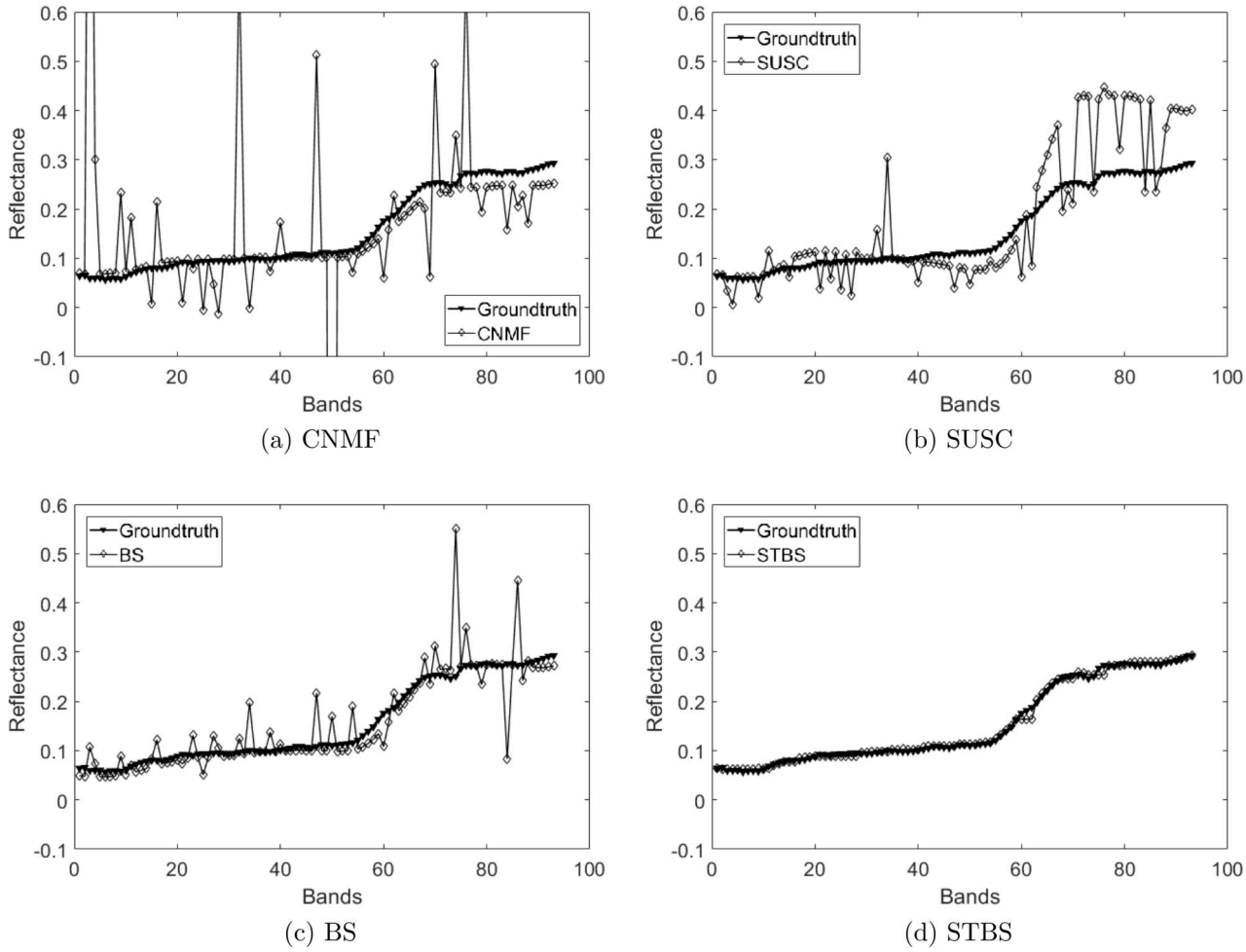

(a) CNMF (b) SUSC

(c) BS (d) STBS

Figure 4: Reconstructed spectrum using different fusion methods (MN)

method on classification accuracy is also investigated. The subset of Pavia dataset contains a groundtruth (labeled training set are available), including six classes (asphalt, meadows, trees, painted metal sheets, self-blocking bricks and shadow). Ten samples of the available labeled samples for each class are randomly selected for training. The support vector Machin (SVM)[23] classifier is used in order to classify the fused datasets. The average accuracy (AA) for each class and overall accuracy (OA) and kappa coefficient of the classified fused images for various fusion methods are reported in Table.2. Since SVM is not robust, for each fused data, accuracy measurements (OA, AA and kappa) are calculated 40 times and the reported values are the averaged measurements over all values. Figures.5 & 6 show the obtained classification maps. The applied SVM algorithm is taken from the LIB-SVM toolbox[24] by using the Gaussian kernel with five fold cross-validation. The classification maps for each fused method are depicted in figures.5 & 6 in order to visually compare the classification results for HRHSI affected by high Gaussian noise and MN respectively.

4. CONCLUSIONS

In this paper, the effect of HSI denoising on fusion of LRHSI with MSI is investigated. First, the existing LRHSI is denoised using shearlet transform method. After that, the fusion problem is solved by Bayesian sparse method. The visual and qualitative fusion results show that the proposed method (STBS) significantly enhances the spatial resolution of HSI with low spectral distortion compared to state-of-the-art reconstruction based on

Table 2: SVM classification results

Class		Data		AA (high Gaussian noise)$_{(\%)}$				AA (MN)$_{(\%)}$			
Number	*Name*	*Train*	*Test*	**CNMF**	**SUSC**	**BS**	**STBS**	**CNMF**	**SUSC**	**BS**	**STBS**
1	**Asphalt**	10	2583	71.97	84.89	80.55	**87.19**	55.32	80.19	81.96	**87.48**
2	**Meadows**	10	4929	75.42	86.97	84.84	**91.10**	69.76	85.72	81.97	**91.04**
3	**Trees**	10	1017	68.69	84.69	78.26	**89.55**	48.36	84.90	82.99	**89.20**
4	**Pianted metal sheets**	10	1118	63.94	**96.40**	92.32	86.10	46.67	**89.92**	89.37	89.00
5	**Self blocking bricks**	10	1105	86.64	90.77	86.90	**95.24**	63.52	89.12	87.67	**94.25**
6	**Shadow**	10	155	98.42	99.08	96.63	**99.37**	96.82	98.11	92.77	**99.37**
OA$_{(\%)}$				74.26	87.79	84.35	**90.06**	61.73	85.28	83.56	**90.26**
Kappa				0.656	0.833	0.788	**0.863**	0.483	0.800	0.779	**0.866**

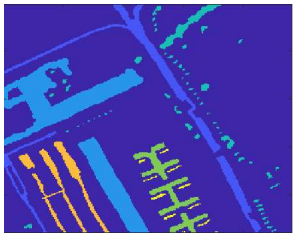

(a) Groundtruth

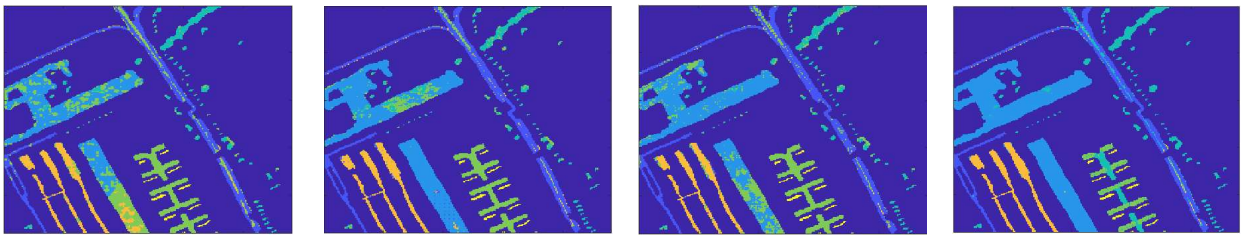

(b) CNMF (c) SUSC (d) BS (e) STBS

Figure 5: Classification maps of different classified HRHSI (high Gaussian noise)

spectral unmixing and sparse code in the presence of high Gaussian noise and Spike noise. The performance of the other fusion methods is decreased by mixture noise a lot. Therefore, the denoising of HSI is suggested before fusion of HSI and MSI.

REFERENCES

1. Wei, Q., Bioucas-Dias, J., Dobigeon, N., and Tourneret, J.-Y., "Hyperspectral and multispectral image fusion based on a sparse representation," *IEEE Transactions on Geoscience and Remote Sensing* **53**(7), 3658–3668 (2015).

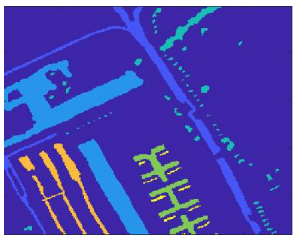

(a) Groundtruth

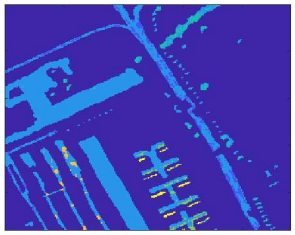

(b) CNMF

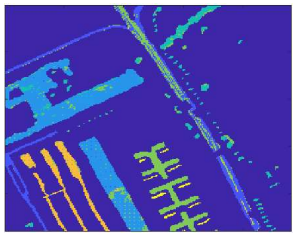

(c) SUSC

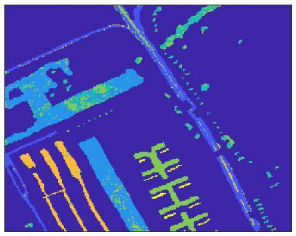

(d) BS

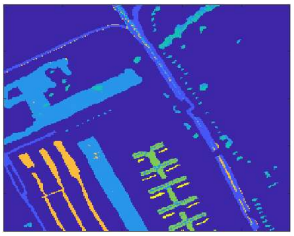

(e) STBS

Figure 6: Classification results of different classified HRHSI (MN)

2. Yang, J., Li, Y., Chan, J. C.-W., and Shen, Q., "Image fusion for spatial enhancement of hyperspectral image via pixel group based non-local sparse representation," *Remote Sensing* **9**(1), 53–72 (2017).
3. Heylen, R., Burazerovic, D., and Scheunders, P., "Fully constrained least squares spectral unmixing by simplex projection," *IEEE Transactions on Geoscience and Remote Sensing* **49**(11), 4112–4122 (2011).
4. Yokoya, N., Yairi, T., and Iwasaki, A., "Coupled non-negative matrix factorization for hyperspectral and multispectral data fusion: Application to pasture classification," in [*Geoscience and Remote Sensing Symposium (IGARSS), 2011 IEEE International*], 1779–1782, IEEE (2011).
5. Wei, Q., Bioucas-Dias, J., Dobigeon, N., Tourneret, J.-Y., Chen, M., and Godsill, S., "Multiband image fusion based on spectral unmixing," *IEEE Transactions on Geoscience and Remote Sensing* **54**(12), 7236–7249 (2016).
6. Nezhad, Z. H., Karami, A., Heylen, R., and Scheunders, P., "Superresolution of hyperspectral images using spectral unmixing and sparse regularization," in [*Geoscience and Remote Sensing Symposium (IGARSS), 2016 IEEE International*], 7216–7219, IEEE (2016).
7. Licciardi, G., Veganzones, M. A., Simoes, M., Bioucas-Dias, J. M., and Chanussot, J., "Super-resolution of hyperspectral images using local spectral unmixing," in [*IEEE Workshop on Hyperspectral Image and Signal Processing: Evolution in Remote Sensing (WHISPERS 2014), Lausanne, Switzerland, 25–27 June 2014*], 1–4 (2014).
8. Akhtar, N., Shafait, F., and Mian, A., "Sparse spatio-spectral representation for hyperspectral image super-resolution," in [*European Conference on Computer Vision*], 63–78, Springer (2014).
9. Ghasrodashti, E. K., Karami, A., Heylen, R., and Scheunders, P., "Spatial resolution enhancement of hyperspectral images using spectral unmixing and bayesian sparse representation," *Remote Sensing* **9**(6), 541–561 (2017).
10. Majumdar, A., Ansari, N., Aggarwal, H., and Biyani, P., "Impulse denoising for hyper-spectral images: A blind compressed sensing approach," *Signal Processing* **119**, 136–141 (2016).
11. Aggarwal, H. K. and Majumdar, A., "Hyperspectral unmixing in the presence of mixed noise using joint-sparsity and total variation," *IEEE Journal of Selected Topics in Applied Earth Observations and Remote Sensing* **9**(9), 4257–4266 (2016).
12. Chen, C., Li, W., Tramel, E. W., Cui, M., Prasad, S., and Fowler, J. E., "Spectral–spatial preprocessing using multihypothesis prediction for noise-robust hyperspectral image classification," *IEEE journal of selected topics in applied earth observations and remote sensing* **7**(4), 1047–1059 (2014).

13. Zhang, Z., Pasolli, E., Crawford, M. M., and Tilton, J. C., "An active learning framework for hyperspectral image classification using hierarchical segmentation," *IEEE Journal of Selected Topics in Applied Earth Observations and Remote Sensing* **9**(2), 640–654 (2016).
14. Karami, A., Heylen, R., and Scheunders, P., "Denoising of hyperspectral images using shearlet transform and fully constrained least squares unmixing," in [*IEEE Whispers 2016: Workshop on Hyperspectral Image and Signal Processing: evolution in remote sensing, 21-24 August 2016, Los Angeles*], 1–5 (2016).
15. Wang, W. and He, C., "A fast and effective algorithm for a poisson denoising model with total variation," *IEEE Signal Processing Letters* **24**(3), 269–273 (2017).
16. Karami, A., Heylen, R., and Scheunders, P., "Band-specific shearlet-based hyperspectral image noise reduction," *IEEE Transactions on Geoscience and Remote Sensing* **53**(9), 5054–5066 (2015).
17. Miao, Q., Liu, R., Quan, Y., and Song, J., "Remote sensing image fusion based on shearlet and genetic algorithm," *International Journal of Bio-Inspired Computation* **9**(4), 240–250 (2017).
18. Nascimento, J. M. and Dias, J. M., "Vertex component analysis: A fast algorithm to unmix hyperspectral data," *IEEE transactions on Geoscience and Remote Sensing* **43**(4), 898–910 (2005).
19. Hardie, R. C., Eismann, M. T., and Wilson, G. L., "Map estimation for hyperspectral image resolution enhancement using an auxiliary sensor," *IEEE Transactions on Image Processing* **13**(9), 1174–1184 (2004).
20. Mairal, J., Bach, F., Ponce, J., and Sapiro, G., "Online dictionary learning for sparse coding," in [*Proceedings of the 26th annual international conference on machine learning*], 689–696, ACM (2009).
21. Tropp, J. A. and Gilbert, A. C., "Signal recovery from random measurements via orthogonal matching pursuit," *IEEE Transactions on information theory* **53**(12), 4655–4666 (2007).
22. Figueiredo, M. A., Bioucas-Dias, J. M., and Afonso, M. V., "Fast frame-based image deconvolution using variable splitting and constrained optimization," in [*Statistical Signal Processing, 2009. SSP'09. IEEE/SP 15th Workshop on*], 109–112, IEEE (2009).
23. Melgani, F. and Bruzzone, L., "Classification of hyperspectral remote sensing images with support vector machines," *IEEE Transactions on geoscience and remote sensing* **42**(8), 1778–1790 (2004).
24. Chang, Chih-Chung, Lin, and Chih-Jen, "Libsvm: A library for support vector machines," *ACM Transactions on Intelligent Systems and Technology,* **2**(3), 1–27 (2011). http:/www.csie.ntu.edu.tw/ cjlin/libsvm.